Published in final edited form as:
IEEE Trans Ultrason Ferroelectr Freq Control. 2007 September ; 54(9): 1772–1783.

A Computer-Controlled Ultrasound Pulser-Receiver System for Transkull Fluid Detection using a Shear Wave Transmission Technique

Sai Chun Tang, **Gregory T. Clement**, and **Kullervo Hynynen**

Abstract

The purpose of this study was to evaluate the performance of a computer-controlled ultrasound pulser-receiver system incorporating a shear mode technique for transkull fluid detection. The presence of fluid in the sinuses of an ex vivo human was examined using pulse-echo method by transmitting an ultrasound beam through the maxilla bone towards the back wall on the other side of the sinus cavity. The pulser was programmed to generate bipolar pulse trains with 5 cycles, at frequency of 1MHz, repetition frequency of about 20Hz, and amplitude of 100V to drive a 1MHz piezoelectric transducer. Shear and longitudinal waves in the maxilla bone were produced by adjusting the bone surface incident angle to 45° and 0°, respectively. CT scans of the skull were performed to verify the ultrasound experiment. Using the shear mode technique, the echo waveform clearly distinguishes the presence of fluid, and the estimated distance of the ultrasound traveled in the sinus is consistent with the measurement from the CT images. Contrarily, using the longitudinal mode, no detectable back wall echo was observed under the same condition. As a conclusion, this study demonstrated that the proposed pulser-receiver system with the shear mode technique is promising for transkull fluid detecting, such as mucous in sinus.

I. Introduction

Sinusitis, or sinus infection, which can be caused by a number of conditions, and is one of the most common healthcare problems in the U.S., accounting for more than $5.8 billion in direct health care expenditures [1-4]. Acute bacterial infection occurs when bacteria colonize and overgrow in trapped fluid in the sinuses, [5-7] generally indicating the need for treatment with antibiotics. However, up to 98% of cases of sinusitis are viral, and can generally be treated with over the counter medications. Despite this, primary care physicians prescribe antibiotics for up to 85% to 98% of patients suspected to have rhinosinusitis [3].

To differentiate between viral and bacterial infection, the presence of an air-fluid level in the maxillary sinus [8-9], as assessed by puncture or imaging, provides a standard for evaluating the diagnostic reliability of physical symptoms. The absence of these findings is highly significant for ruling out bacterial infection. Therefore plain X-ray radiographs or computed tomography is used to evaluate the presence of fluid. Unfortunately, the cost and convenience of both approaches cost have been an obstacle to its routine use for diagnosis.

The potential for ultrasonic pulse-echo A-scan to detect transkull fluid, such as mucous in sinus, has been realized for more than three decades [10]-[15]. In ultrasound diagnosis of sinusitis, high amplitude acoustic pulse is transmitted through the maxilla bone towards the back wall of the sinus cavity on other side of the bone. The air in a normal sinus prevents the ultrasound propagation; only one echo from the front wall of the sinus is produced. On the other hand, if the sinus is infected, the sinus will be filled with fluid that conducts the ultrasound and a second echo from the back wall will be generated [16].

Unfortunately, significant variability in the method results from strong ultrasound scattering and attenuation caused by the skull. In previous ultrasonic sinus fluid detection studies [17], [18], the ultrasound transducer was placed parallel to the maxilla bone and the incident angle was approximately zero degree. The problem of using such a configuration is two-fold. Firstly, the ultrasound propagation inside the bone is primarily in longitudinal mode [19], [20]. The speed (~2820ms^{-1}) of longitudinal sound propagation inside skull bone is almost twice of the sound speed in soft tissues and water (~1500ms^{-1}). The large discrepancy in sound speed causes significant impedance mismatch, most of the ultrasound energy is reflected at the boundary between the media. As a result, the ultrasound energy transmitted through the bone is greatly reduced. In practice, a very high amplitude acoustic pulse from the transducer is required to compensate for the reflection loss. Secondly, as the transducer is oriented parallel to the bone, multiple reflections between the bone and the transducer may occur. These multiple echoes would deteriorate the signal-to-noise ratio (SNR) of the desired back wall echo signal, and therefore decreases the accuracy of the detection.

Yet, a reliable ultrasound method would have clear advantages over existing standard methods for sinusitis diagnosis, such as sinus puncture and X-ray computer tomography (CT). Ultrasound represents a very compact, low cost method that is non-invasive and does not involve ionizing radiation [17], [21]. It is envisaged that a portable, single channel ultrasound modality would provide a convenient and cost-effective clinical procedure for sinusitis diagnosis, and follow-up of treatment results.

The present work examines an improved method for propagating into the sinuses using a shear mode conversion. Recently, it has been demonstrated that the use of shear wave propagation, instead of longitudinal mode, inside the skull bone can improve ultrasound transmission substantially [19], [20]. The shear wave in skull bone can be produced by adjusting the incident angle greater than the longitudinal critical angle. Unlike the longitudinal mode, the sound speed of shear wave (~1400ms^{-1}) in skull bone is close to that of soft tissues. The similarity in speed of sound improves the acoustic impedance matching considerably, and thus increases the transmitted ultrasound energy through the bone. The enhanced ultrasound transmission reduces the required acoustic pressure and also the energy consumption of the pulser system. Furthermore, when the shear mode method is used, the transducer is oriented at an angle (>30°) with respect to the maxilla bone, the multiple-reflection issue is naturally relieved as a significant portion of the echo from the maxilla bone reflects away from the transducer.

In this study, we developed a compact and economical computer-controlled pulser-receiver system and demonstrated the operation of the system incorporating a shear mode technique derived in our prior studies [19], [20]. The purpose of this study was to investigate the performance of the system using the shear mode method and compare with its traditional counterpart, longitudinal mode for transcranial fluid detection using an *ex vivo* human skull.

II. Pulser-receiver system design

A block diagram of the proposed ultrasonic pulser-receiver system is shown in Fig. 1. Both transmitting ultrasound pulses and receiving echo signal are accomplished by the same transducer. The transducer is driven by a pulse train generator, which delivers high-voltage bipolar pulse train. Bipolar voltage pulse is employed because it has lower unwanted DC and low-frequency component that may increase the leakage current compared to its unipolar counterpart. Another advantage of using bipolar pulse is that the peak-to-peak pulse voltage can be twice the voltage rating of the coaxial cable connecting the pulser and the transducer. As a result, the size and cost of the cable can be substantially reduced, especially in the case when multi-element transducer array is used.

The amplitude of the pulse train is determined by the output voltage of the high-voltage DC supply, which steps up battery voltage (e.g. 12V) to ±60-180VDC. The amplitude and the signal-to-noise-ratio (SNR) of the received echo signal can be improved by increasing the pulse train amplitude and driving the transducer at its resonance frequency. The frequency of the pulse train can be either generated by a computer through a digital I/O interface or from an external signal source such as a function generator or an oscillator. In the prototype design, the pulse train is generated by a digital I/O card (PCI6534, National Instruments, Austin, TX). The pulse frequency and number of pulses are programmed by a personal computer with a program implemented by LabVIEW (National Instruments, Austin, TX).

On the receiving side, the echo ultrasonic signal is converted to an electrical signal by the same transducer, and amplified by a high-gain amplifier. High-pass filters are integrated in the echo amplifier to eliminate the low repetition frequency, which might saturate the high-gain amplifier. The amplified echo signal is then converted to digital format by a high-speed analog-to-digital converter (ADC). This digitized echo data is temporarily stored in the on-board memory and then transferred to the personal computer that stores and analyzes the signal.

A. High-voltage DC supply

A high-voltage pulse train for driving the transducer is desired to produce large-amplitude ultrasound and improve the SNR of the echo signal. The bipolar pulse train amplitude at the pulse generator output follows the output voltages (±HV) of the high-voltage DC power supply. Fig. 2 shows the circuit diagram of the dual high-voltage power supply. The positive and negative output voltages designated as +HV and −HV, respectively, are variable from ±60V to ±180V. High voltage is accomplished by employing a high-turns-ratio step-up transformer (Tr_1). The power converter is connected in flyback topology. The output voltage and power is controlled by the duty ratio of the metal-oxide-semiconductor field effect transistor (MOSFET) Q_1. When Q_1 is turned-on, current flows into the primary of Tr_1. Diodes D_1 and D_2 are reverse-biased, so secondary windings are open-circuited. At this state, magnetic energy is stored in the transformer core, and no energy transfers to the secondary side. When Q_1 is turned-off, back electromotive force (EMF) is induced at the secondary windings, and magnetic energy stored in the transformer is released to the secondary side. At this state, D_1 and D_2 are forward-biased. Capacitors C_1 and C_2 are being charged towards the desired voltage level, which is controlled by a MOSFET controller LM3478 (National Semiconductor, Santa Clara, CA). This controller uses current mode control scheme to limit the MOSFET (Q_1) and output currents by feeding the voltage across the current sensing resistor (R_S) into the current sensing pin I_{sen}. The output voltage is sensed through a feedback resistor divider network (R_1, R_2 and VR_1) and fed into the feedback pin (FB) of the controller. The positive output voltages, +HV, can be controlled between 60V and 180V by adjusting the position of potentiometer VR_2. The lower and upper voltage limits are determined by the values of resistors R_1 and R_2. With the information of the feedback voltage and current, driving signal for Q_1 with appropriate duty cycle can be generated by the controller. By transforming the feedback resistor divider network to its equivalent circuit as shown in Fig. 3, the output voltage is giving by [22]:

$$+HV = 1.26\left(1 + \frac{R_A}{R_B}\right) \quad (1)$$

Because the pulse generator loads the positive and negative outputs symmetrically, the negative voltage amplitude follows the positive voltage level, and therefore both voltages can be regulated using the same controller. The resistor, R_3, connected to the negative output terminals is used to discharge the high-voltage across C_2 when the circuit is turned-off for the sake of safety. It also balances the load at the positive and negative outputs in order to keep the dual voltage amplitude symmetric.

The high-voltage DC supply operates as a switching mode power converter that could be a significant source of electromagnetic interference (EMI) to the very sensitive high-gain echo amplifier. For this reason, the high-voltage power supply is shut down temporary at the period between sending pulse train and waiting for echo signal by applying logic low-level signal to the high-voltage-enable (HVEN) input. During this period, the output capacitors C_1 and C_2 supply energy to the pulse generator. In the circuit prototype, ripple voltage less than 0.1% of the output voltage was measured when both of C_1 and C_2 are 1μF and the idle time is 100μs.

B. Pulse generator

Similar to the high-voltage supply, the design of the pulse train generator was configured to operate at switching mode so as to minimize the power consumption and heat dissipation. Without the requirement of cooling, the cost, size and weight of the pulse train generator are significantly reduced. Moreover, reliability and accuracy can be considerably improved as there is no excessive heat generated from the circuit. The driving circuit for the transducer, as shown in Fig. 4, is made of a half-bridge switching converter. The dual voltage supply ±HV determines the amplitude of the bipolar pulse train, which is generated by switching on-and-off the N-channel power MOSFETs Q_3 and Q_4 complementarily. In the positive half-cycle, Q_3 is on and $Q_4$is off, the generator output voltage equals to +HV. On the contrary, during the negative half-cycle,Q_3 is off and Q_4 is on, and the output voltage becomes −HV.

In the design of a practical pulse generator, parasitic capacitors associated with the MOSFETs and the coaxial cable connecting to the transducer have to be considered. These capacitors keep the pulse generator output at high voltage for a long period that could saturate the high-gain echo amplifier and also increase the leakage current that may create safety issues. Thus, at the end of each pulse train, discharging the parasitic capacitors to zero potential is essential. The purpose of solid-state switch S_1 is to discharge the parasitic capacitors when both of Q_3 and Q_4 are in the off-state. Fig. 5 illustrates the solid-state switch that discharges the parasitic capacitor, via MOSFET Q_5 and Q_6. The operating principle of this solid-state switch is detailed in [23].

The gating signals for Q_3, Q_4 and S_1 are generated by the computer I/O interface with software control, although we have verified they could be achieved by standalone digital circuitry. Because the source terminals of both Q_3 and Q_4 are not connected to the ground, isolated gate drive circuits for the MOSFETs are required. In this prototype, isolation is achieved by using a signal transformer T_{r2} with two secondary windings and turns ratio of 10:15:15.

C. Echo amplifier

In practical situations, the received echo signal intensity can be less than 1% of that sending out from the transducer. A high gain amplifier is required to amplify the echo signal received from the transducer. The echo amplifier being used consists of four stages of low-noise operational amplifiers, OA_1 to OA_4, as shown in Fig. 6. Each stage provides voltage gain of 10 times, and 10^4 times in total. Two first-order high-pass filters (HPFs) are integrated into the amplifier circuit to eliminate the low repetition frequency, which may cause the amplifier saturated. The coarse and fine gain adjustments of the amplifier are accomplished by potentiometers VR_2 and VR_3, respectively. Because the echo amplifier input is connected directly to the pulse generator output that delivers high-voltage pulse train, a protection scheme is necessary to prevent the echo amplifier from damaging by the high voltage. At the echo amplifier input, the non-inverting input of OA_1 is limited to less than one volt by using two inexpensive small signal diodes (D_4 and D_5) in anti-parallel connection.

D. Analog-to-digital converter and memory

The amplified echo signal is converted to digital format by a high-speed analog-to-digital converter (AD9215, Analog Devices, Norwood, MA) as shown in Fig. 7. The sampling frequency of data conversion is set to 66.67 Mega-samples per second (MSPS). In order to achieve optimum signal conversion performance, the single-ended amplified echo signal is converted to differential format by signal transformer Tr_4, and filtered by a pair of RC low-pass networks [24]. The digital output from the ADC is connected to the data I/O pins (D_0-D_9) of the memory via an array of switches S_2, which controls the data flow from the ADC to the memory. The switches turn on only when the echo signal is being recorded to the memory.

Because of the high sampling rate of the data conversion, a high-speed static random-access memory (SRAM) (K6R1016V1D, Samsung Semiconductor Inc., San Jose, CA) is employed to cache the digitized echo signal. This SRAM is a 64kB, 16-bit, high-speed memory with up to 8ns access time. After a whole frame of analog echo signal is digitized and cached in the SRAM, the data in the SRAM will be transferred to a PC through the digital I/O card PCI6534 for storage and analysis. The memory addressing of the SRAM is controlled by a high-speed 16-bit counter. The triggering of the data conversion, data flow direction and the memory address counting are controlled by the LabVIEW program through the same digital I/O card.

III. Experiment

A. Sinus fluid detection setup

The use of the ultrasonic pulser-receiver system for the detection of fluid in sinus cavities is illustrated in Fig. 8. The presence of fluid in the maxillary sinuses of an *ex vivo* human skull was being detected. An ultrasound simulation study was conducted with a previously described transkull ultrasound propagation algorithm, using MRI sinus images of a volunteer in order to determine the optimal transducer frequency, diameter, and radius of curvature. In this study, ultrasound was propagated first as a longitudinal signal that was then separated into both a longitudinal and shear mode in the bone. Both modes then transferred back to two longitudinal signals in the fluid filled sinus. This signal was reflected off the back wall of the sinus, where the mode conversion reoccurred as the signal exited the head. Based on this study, a 1MHz-resonance PZT crystal (EBL, East Hartford, CT) was selected, with 20 mm diameter, and 40 mm radius of curvature. The crystal backed with 25% tungsten-epoxy composite material for acoustic damping, and mounted so that the ultrasound is directed at an angle of approximately 45° relative to the skull surface. The beam width at the point of contact with the mandible is elongated due to the angle of incidence, entering with an approximately 10 mm × 7 mm footprint on the mandible surface.

For the study, a human skull was a reconstituted after full desiccation by submersing it in deionized water and degassing the specimen in a bell jar. Afterward, the skull was stored in a 10% buffered formaldehyde solution. A previous study has shown that human skulls undergoing this dehydration-reconstitution process have sound speeds closely matching that of fresh bone tissues [25].

The transducer and human skull were immersed in degassed de-ionized water in a tank filled with padded rubber to reduce reflections from the tank walls. The detections of fluid in both left and right maxilla sinus cavities were performed. For the experiments of sinus fluid detection, the sinus cavity was first completely filled with water. Control experiments were conducted by inserting a tube into the sinus cavity and injecting air with a syringe attached to the other end of the tube. The skull was oriented with the face horizontal in order to trap the air in the sinus for the control experiments.

The effects of shear and longitudinal propagation through the maxilla bone were examined by orienting the transducer at different angles as shown in Fig. 9. For the measurement of the echo signal with shear mode propagation through the maxilla bone, the incident angle was adjusted to approximately 45°, which is greater than the longitudinal critical angle of about 30° [19]. It is noted that both the transmitted and received wave was longitudinal. The propagation involved a mode conversion from longitudinal in the skin into a shear wave in the bone, and then back into longitudinal in the sinus fluid, if present. If the cavity was fluid-filled, the reverse process took place where echoes off of the back of the sinus cavity were again converted to shear waves in the bone and then back to longitudinal before reaching the transducer. For the echo measurement associated with longitudinal propagation in bone, the transducer is positioned approximately parallel to the maxilla bone, so that the incident angle (~0°) is smaller than the longitudinal critical angle.

B. Pulser-receiver system

The computer-controlled ultrasonic pulser-receiver system described in the previous section was constructed in-house. The pulser-receiver system was used to transmit high-voltage pulse train to and receive echo signal from the same transducer. The transducer was connected to the pulser-receiver through a Belden 8216 RG174U 50Ω coaxial cable of length about 1m. Bipolar pulse train with amplitude regulated at ±100V is adopted to excite the transducer. The pulse train frequency of 1MHz and five pulse cycles in each pulse train were set through a software interface, implemented in LabVIEW code, as shown in Fig. 10. At the end of each pulse train, the pulser output was shorted to ground for 10μs to discharge the undesired stray capacitor formed by the pulser output MOSFETs, coaxial cable and the transducer.

Both pulse train transmission and echo receiving were controlled using the same software interface. The voltage across the transducer terminals was sensed, recorded and transmitted to the computer in real time. Data recording started when the pulse train was transmitted, and the record duration was set to 100μs. The sensed transducer voltage was converted to 10-bit digital offset binary format, buffered in a static RAM, and then transmitted to a PC at a rate of 20Mbytes/s. Signal process for the received transducer voltage was handled by a 6^{th}-order software Butterworth low-pass-filter implemented in LabVIEW code in order to filter out high frequency noise. The cut-off frequency was set to 3.4MHz. The repetition frequency of the pulse train and data conversion/recording cycle was approximately 20Hz. Real-time transducer voltage waveform was displayed on the software interface for the measurements of time-of-fight, and hence the distance between the objects that the ultrasound beam traveled. The echo waveforms for the experiments were saved in the computer hard disk for further analysis.

C. Sinus imaging

Structure and dimensions of the maxilla bone of the *ex vivo* human skull used in the sinus fluid detection experiment were obtained by computed tomography (CT) images (Somatom Sensation 64, Siemens, Erlangen, Germany). The skull was preserved in formalin and scanned under water. Two hundred CT slides in coronal view were taken at 1mm intervals using a 279×279-mm field of view with resolution of 512×512-pixel (0.54 mm^2 pixels). Image data for each slide was saved to an individual file in binary format. Axial and sagittal views of the skull were reconstructed (Fig. 11) from the coronal view image files using a program (written in-house) implemented by LabVIEW code with embedded MATLAB script.

IV. Results

The transducer signals recorded by the pulser-receiver system for sinus fluid detection are shown in Figs. 12-13. It should be noted that, first, a high-amplitude voltage swing with a duration of a few micro-second at the beginning of every recorded signal was caused by the

coupling from the high-voltage pulse train originated from the pulse generator. Second, a short period of voltage swing appeared at around 15-16μs was caused by the transducer transient when the solid-state-switch connected the transducer and the ground was opened. Thus, the receiver began to receive echo signal after the settling of the transducer transient at around 16μs.

The sagittal views of the CT scans for the *ex vivo* human skull in upside down orientation, showing the left and right maxillary sinuses, are displayed in Figs. 14(a) and (b), respectively. The positions of the transducer for the shear mode experiment are indicated on the figures. For the case of shear wave propagation, the transducer voltage signals from the left and right sinuses filled with air and water are shown on Figs. 12 (a)-(d), respectively. In this case, the ultrasound beam first hit the outer surface of the maxilla bone (indicated by ①), as illustrated in Figs. 14 (a) and (b). This echo propagated back to the transducer surface at about 18μs after transmitting the pulse train as shown in Fig. 12. When the sinus cavity is filled with water, the ultrasound beam then transmitted through the sinus and hit the back wall of the maxilla bone as indicated by ② in Figs. 14(a) and (b). The second echo propagated back to the transducer surface at around 40μs as shown in Figs. 12(a) and (b). Conversely, when the sinus is filled with air, the ultrasound beam was reflected back at the first hit and could not transmit through the air sinus due to impedance mismatch. Figs. 12(c) and (d) reveal that the received transducer signal had only one echo for the air-filled sinus.

As indicated on the CT images in Fig. 14, the shapes of the left and right maxilla bones are not identical. Echo signal measurements, in Figs. 12(a) and (b), also show that the echo amplitudes from the second reflection on the left and right maxilla bones are not the same. The ratio between the second echo and the noise amplitudes on the left and right sides are 3.3 and 13.9, respectively. However, the echo times are approximately the same on both sides. Based on the measured echo time, the distance between points ① and ② in both sinuses are approximately 16.5mm, with the assumption that the sound speeds in water and the bone in shear mode [19] are both $1500 ms^{-1}$. The distance estimation is found to be consistent with the measurement from CT scan, as illustrated in Fig. 14.

The effect of longitudinal wave propagation in bone was examined by orienting the transducer in parallel to the maxilla bone. In this case, the incident angle was approximately zero degree and smaller than the longitudinal critical angle of skull [19]. Measured transducer voltage waveforms for longitudinal propagation on both left and right maxillary sinuses filled with water and air are displayed in Fig. 13. For all of these cases, only one echo from the maxilla bone was received at 18μs.

V. Discussion

This study confirms our previous investigations on transkull ultrasound transmission enhancement using shear mode conversion, in which the transmitted ultrasound intensity is increased, and distortion reduced by improved acoustic impedance matching. In this study, we developed a self-contained clinical prototype of ultrasonic pulser-receiver system with computer control for transkull fluid detection. Incorporating the shear mode technique, we demonstrated that the system could be used to distinguish the presence of fluid in sinus cavities in an *ex vivo*human skull, while the traditional longitudinal method cannot detect with the same pulse voltage.

The pulser-receiver system, built in-house, generates multi-cycle pulse train, instead of a single negative pulse used in traditional pulsers, for transducer excitation delivers higher transmitted ultrasound energy that would increase the echo signal level for SNR improvement. The pulse train frequency was selected to match the transducer resonant frequency at which the transducer

efficiency is optimized. The number of cycles lower limit is determined by the transducer time response when the generated ultrasound amplitude becomes reaching its steady-state value, while the upper limit is limited by the distance between the transducer and the first object hit by the ultrasound beam. Though the pulser can generate pulse amplitude up to 180V, we found that pulse train with 5 cycles, 100V pulse amplitude was enough to obtain a back wall echo with sufficiently high amplitude that could distinguish the presence of fluid in an *ex vivo* human sinus using the shear mode method. The number of pulse cycles and pulse amplitude values were not optimized in this study; they can be further reduced by increasing the gain of the echo amplifier and optimizing the filters parameters. The frequency of the pulse train used in the experiment was 1MHz that is within the appropriate frequency range for ultrasonic transkull diagnostic imaging [26]. Frequency lower than 1MHz can be used to reduce the attenuation in bone with the expense of lower spatial resolution. In this study, the echo signal was digitized by a high sampling rate (66.67MSPS) and high resolution (10-bit) ADC and stored in spreadsheet format for clinician's analysis.

In the pulser-receiver system design, both of the high voltage power supply and the pulse generator operate in switching mode which generally results in higher energy efficiency, smaller size and lighter weight compared to linear mode circuits. The issues due to the parasitic capacitor at the pulser output, the transducer, and the coaxial cable connected between them were considered. A solid-state-switch was used to discharge the high-potential across the capacitor after sending pulses for safety reason. The pulser-receiver system does not generate high temperature; it does not require cooling means, such as heat sink and cooling fan, and works stably throughout our experiments.

From the experimental results of fluid detection using the shear mode technique, the right sinus gave higher back wall echo amplitude than the left though the system parameters, including pulse amplitude and gain of the echo amplifier, were the same. This result was expected and can be explained by the CT images that the left and right sinuses are not symmetric. The area of the right sinus back wall that hit by the ultrasound beam and parallel to the transducer surface is larger than the left. Thus, the amount of ultrasound energy reflected back to the transducer from the right back wall is higher than that from the left at which a significant portion of ultrasound reflects away from the transducer, though in reality the ultrasound transmission is more complicated than the beam illustrated in the principle diagram in Fig.9 due to refraction, geometry and dispersion of ultrasonic beam, as well as scattered reflection from curved surfaces. In these experiments, the transducer angle for the left and right measurements were approximately the same. The amount of ultrasound energy received by the transducer can be increased by using a transducer with larger area or adjusting the transducer position and angle so that maximum echo amplitude is measured. Experimental results also confirm that only one echo occurs when the sinus is filled in air in both cases of shear mode and longitudinal mode propagation.

Our comparison results reveal that ultrasound transmission through the skull bone with shear mode conversion for sinus fluid detection is more efficient than the longitudinal mode in which no detectable back wall echo was observed. Although the attenuation coefficient of shear wave is higher than that of longitudinal wave [19], [20], from the CT scan, the sinus bone is very thin (~1mm), the reflection loss in this application is more significant than the loss due to attenuation. Using the shear mode technique, the back wall echo waveform clearly shows the back wall echo time, and thus the approximate distance between the transducer and the back wall, and that between the front and back sinus walls are 30mm and 16.5mm, respectively, assuming the speed of sound in water and shear wave speed in bone are $1500 ms^{-1}$. These results show consistent with the measurements from the CT images and were expected because the shear wave encounters reduced refraction and temporal distortion due to the similarity between the speed of shear wave in bone and the speed of sound in water.

VI. Conclusion

A computer-controlled ultrasound pulser-receiver system incorporating a shear mode technique was proposed and successfully demonstrated for transkull fluid detection. The presence of fluid in sinuses of an *ex vivo* human was clearly distinguished with using shear wave propagation in skull bone, but the longitudinal method failed to detect with the same pulser parameters.

Acknowledgements

This research was supported by UltraDiagnostics, Inc. and research grant No. R21 EB004353 from the National Institutes of Health. The authors would like to thank Jason White for his assistance in acquiring CT images of the human skull.

Reference

1. Desrosiers M, Klossek JM, Benninger M. Management of Acute Bacterial Rhinosinusitis: Current Issues and Future Perspectives. International Journal of Clinical Practice Feb;2006 60:190–200. [PubMed: 16451293]
2. Gonzales R, Bartlett JG, Besser RE, Cooper RJ, Hickner JM, Hoffman JR, Sande MA. Principles of appropriate antibiotic use for treatment of acute respiratory tract infections in adults: background, specific aims, and methods. Annals of internal medicine March;2001 134:479–486. [PubMed: 11255524]
3. Anon JB, Jacobs MR, Poole MD, Ambrose PG, Benninger MS, Hadley JA, Craig WA, Sinus And Allergy Health Partnership. Antimicrobial treatment guidelines for acute rhino sinusitis. Otolaryngology - head and neck surgery June;2004 130(1 Suppl):1–45. [PubMed: 14726904]
4. Winstead W. Rhinosinusitis. Primary Care; Clinics in Office Practice 2003;30:137–154.
5. Garau J, Dagan R. Accurate Diagnosis and Appropriate Treatment of Acute Bacterial Rhinosinusitis, Minimizing Bacterial Resistance. Clinical therapeutics July;2003 25:1936–51. [PubMed: 12946543]
6. Sinus and Allergy Health Partnership. Antimicrobial treatment guidelines for acute rhinosinusitis. Otolaryngology - head and neck surgery July;2000 123:1–4.
7. Herr, RD.; Joyce, SM. Upper Respiratory Tract Infections. In: Brillman, JC.; Quenzer, RW., editors. Infectious Disease in Emergency Medicine. 2nd Edition. Lipincott-Raven; 1997.
8. Melio, FR. Rosen's Emergency Medicine Current Concepts and Clinical Practice. 70. Mosby: 2002. p. 981-5.
9. Low DE, Desrosiers M, McSherry J, Garber G, Williams JW Jr, Remy H, Fenton RS, Forte V, Balter M, Rotstein C, Craft C, Dubois J, Harding G, Schloss M, Miller M, McIvor RA, Davidson RJ. A practical guide for the diagnosis and treatment of acute sinusitis. Canadian Medical Association journal 1997;156(6 suppl):1–14.
10. Mann W, Beck Chl. Apostolidis Th. Liability of ultrasound in maxillary sinus disease. European Archives of Oto-Rhino-Laryngology March;1977 215:67–74.
11. Jannert M, Adréasson L, Holmer N. Diagnostic Ultrasonography of Paranasal Sinuses. IEEE Ultrasonics Symposium 1982:727–728.
12. Varonen H, Mäkelä M, Savolainen S, Läärä E, Hilden J. Comparison of ultrasound, radiography, and clinical examination in the diagnosis of acute maxillary sinusitis: a systematic review. Journal of Clinical Epidemiology 2000;53:940–948. [PubMed: 11004420]
13. Puhakka T, Heikkinen T, Mäkelä MJ, Alanen A, Kallio T, Korsoff L, Suonpää J, Ruuskanen O. Validity of Ultrasonography in Diagnosis of Acute Maxillary Sinusitis. Archives of Otolaryngology-Head & Neck Surgery December;2000 126:1482–1486. [PubMed: 11115287]
14. Lindbæk M, Hjortdahl P. The clinical diagnosis of acute purulent sinusitis in general practice — a review. British Journal of General Practice June;2002 52:491–495. [PubMed: 12051216]
15. Jansson T, Persson HW, Holmer N, Sahlstrand-Johnson P, Jannert M. Ultrasound Doppler for Improved Diagnosis of Disease in the Paranasal Sinuses. IEEE Ultrasonics Symposium 2005:839–841.

16. Lucchin F, Minicuci N, Ravasi MA, Cordella L, Palu M, Cetoli M, Borin P. Comparison of A-mode ultrasound and computed tomography: detection of secretion in maxillary and frontal sinuses in ventilated patients. Intensive Care Medicine November;1996 22:1265–1268. [PubMed: 9120124]
17. Revonta M, Suonpää J. Diagnosis and follow-up of ultrasonographical sinus changes in children. International Journal of Pediatric Otorhinolaryngology October;1982 4:301–8. [PubMed: 6185449]
18. Luukkala M, Mattila P, Revonta M. Sinuscan, a Hand Held Ultrasonic Unit to Detect Maxillary Sinusitis. IEEE Ultrasonics Symposium 1982:724–726.
19. Clement GT, White PJ, Hynynen K. Enhanced ultrasound transmission through the human skull using shear mode conversion. Journal of the Acoustical Society of America March;2004 115:1356–1364. [PubMed: 15058357]
20. White PJ, Clement GT, Hynynen K. Longitudinal and shear mode ultrasound propagation in human skull bone. Ultrasound in Medicine & Biology July;2006 32:1085–1096. [PubMed: 16829322]
21. Hauman CHJ, Chandler NP, Tong DC. Endodontic implications of the maxillary sinus: a review. International Endodontic Journal 2002;35:127–141. [PubMed: 11843967]
22. National Semiconductor Corporation; 2003. LM3478 High Efficiency Low-Side N-Channel Controller for Switching Regulator.
23. Wood P. Transformer-Isolated Gate Driver Provides very large duty cycle ratios. International Rectifier. Application Note AN-950B
24. 10-Bit, 65/80/105 MSPS, 3 V A/D Converter: AD9215. Analog Devices, Inc.; 2004.
25. White PJ, Palchaudhuri S, Hynynen K, Clement GT. The effects of desiccation on skull bone sound speed. IEEE Transactions on Ultrasonics, Ferroelectrics, and Frequency Control. 2006Submitted to
26. Fry FJ, Barger JE. Acoustical properties of the human skull. Journal of the Acoustical Society of America May;1978 63:1576–1590. [PubMed: 690336]

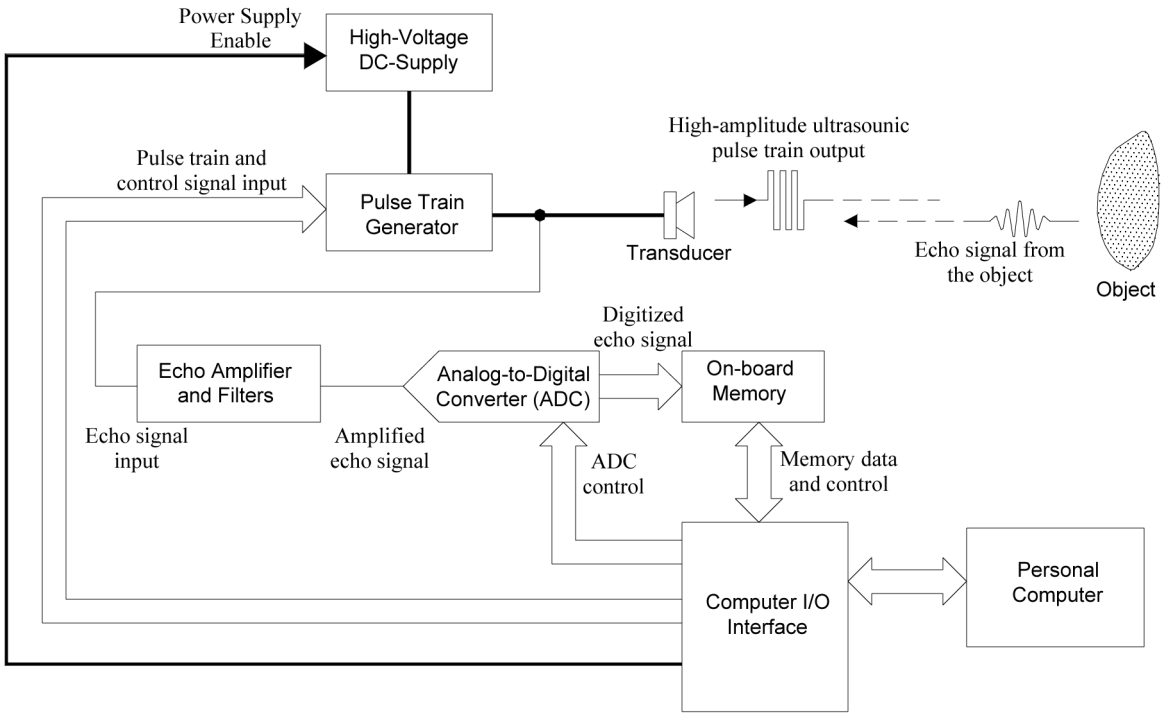

Fig. 1.
A block diagram of the computer-controlled ultrasonic pulser-receiver system

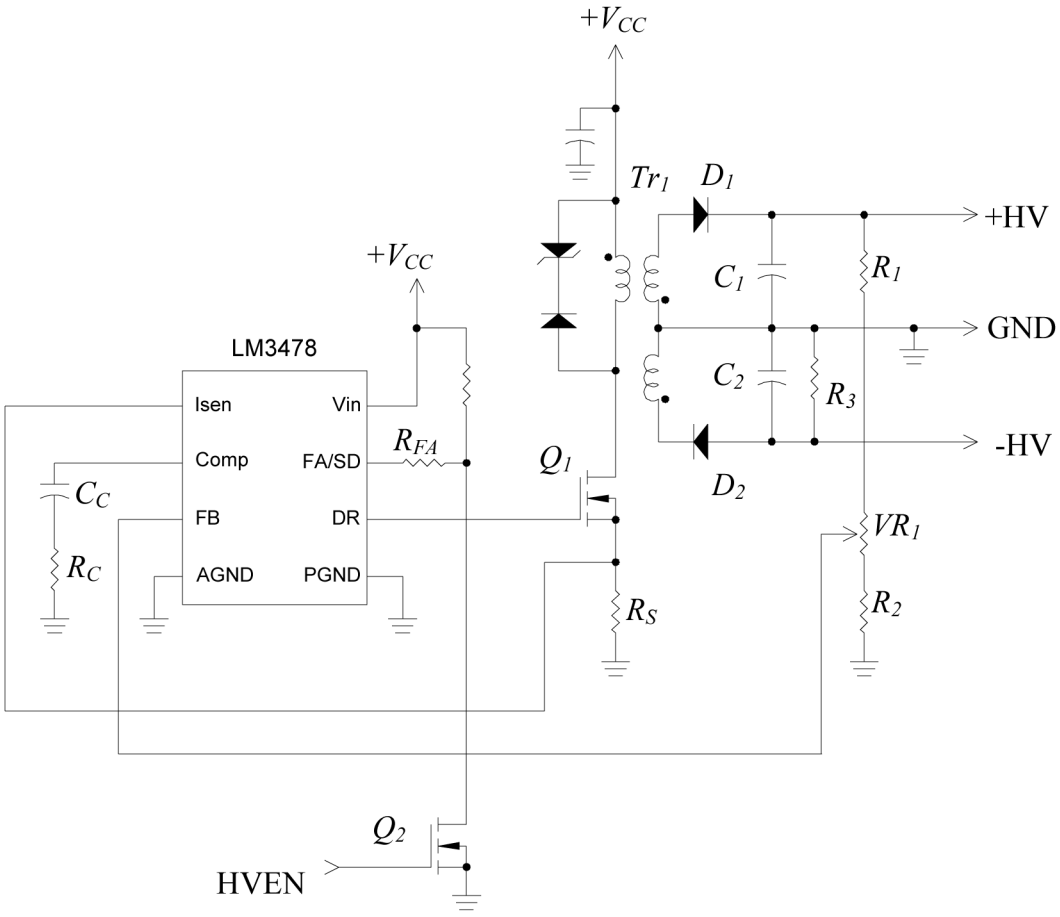

Fig. 2.
Circuit schematic of the high-voltage power supply.

Fig. 3.
Equivalent feedback resistor divider network for the high-voltage power supply.

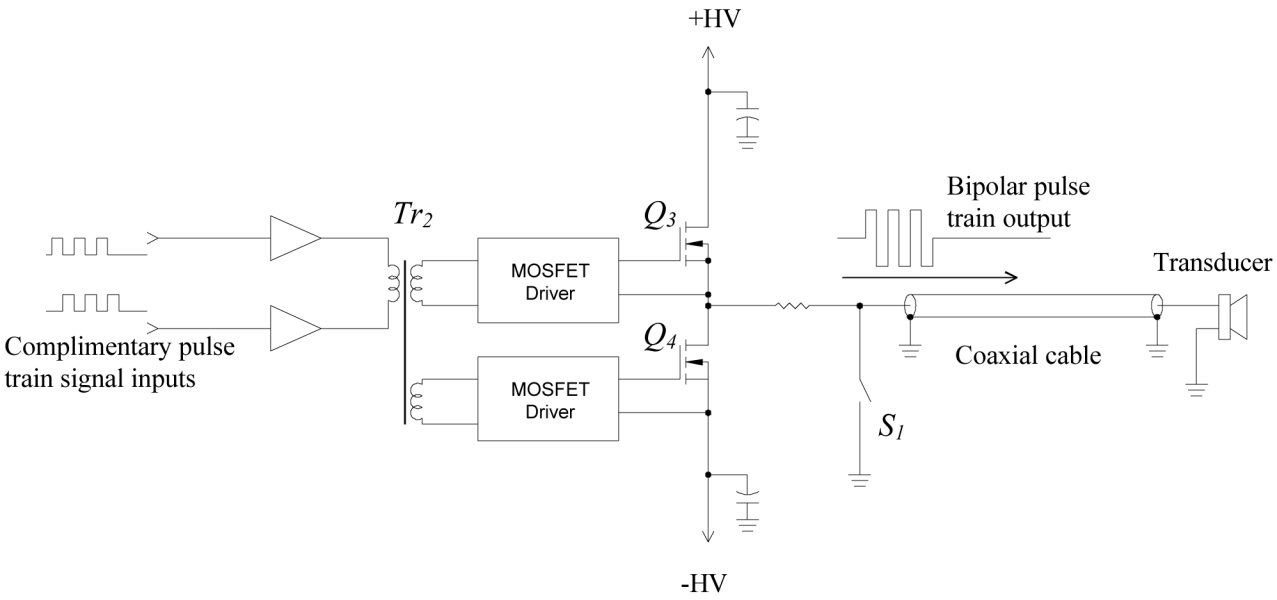

Fig. 4.
Circuit schematic of the pulse generator.

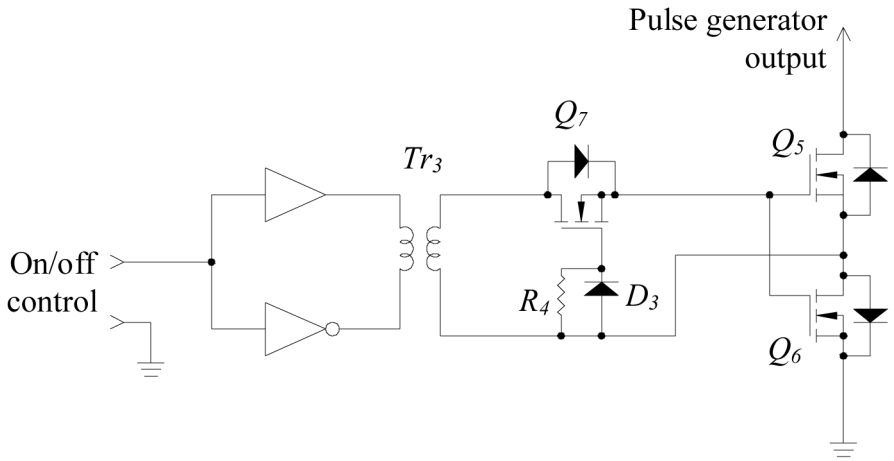

Fig. 5.
Circuit schematic of the solid-state switch, S_1.

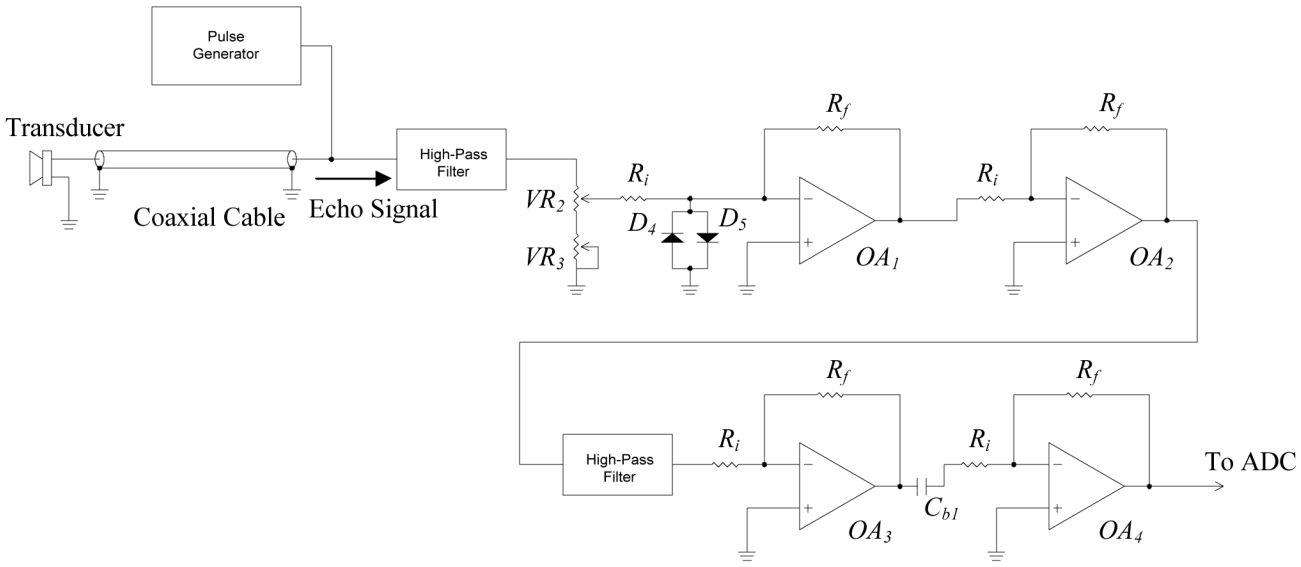

Fig. 6.
Circuit schematic of the echo amplifier.

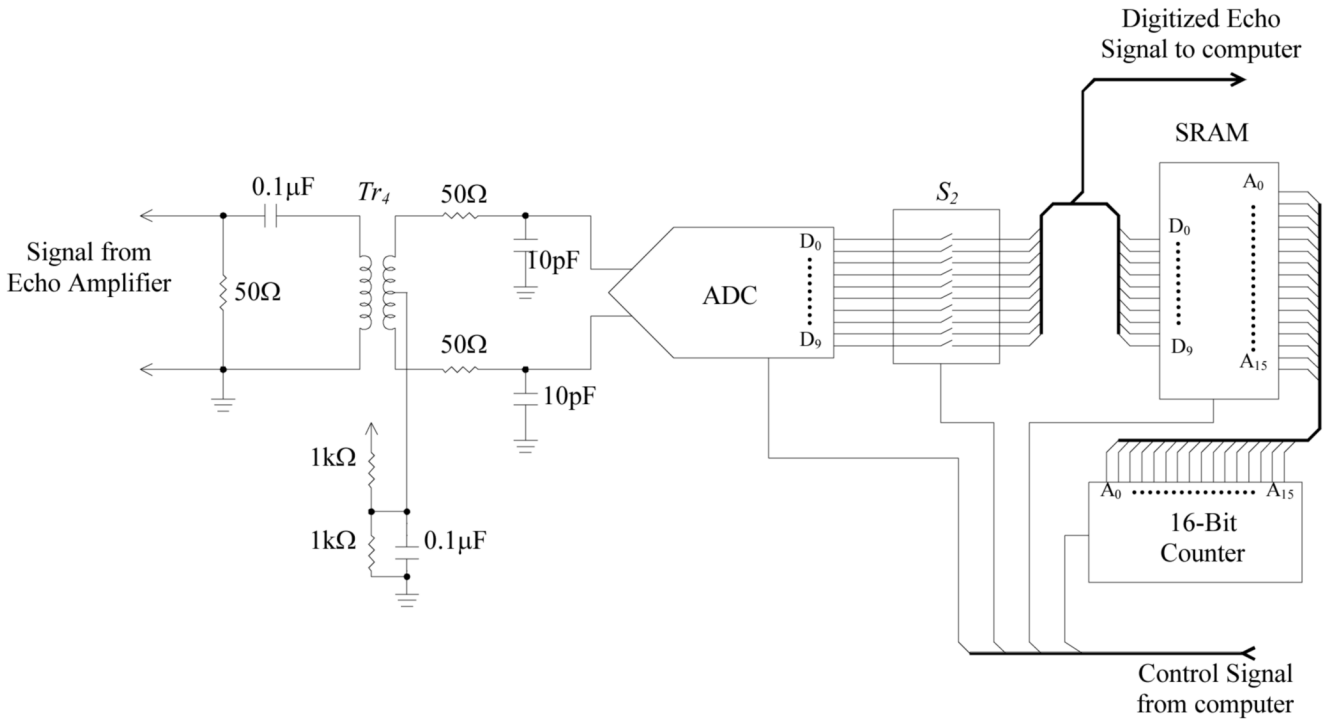

Fig. 7.
Circuit schematic of the analog-to-digital converter and memory.

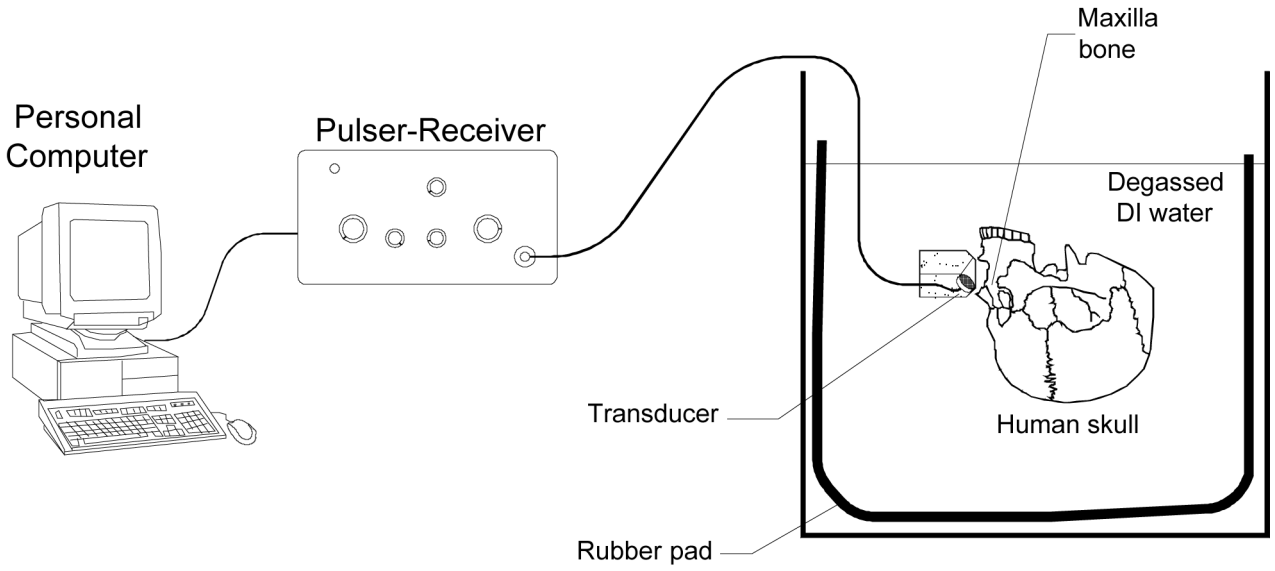

Fig. 8.
Experimental setup for detecting the presence of fluid in the maxillary sinuses.

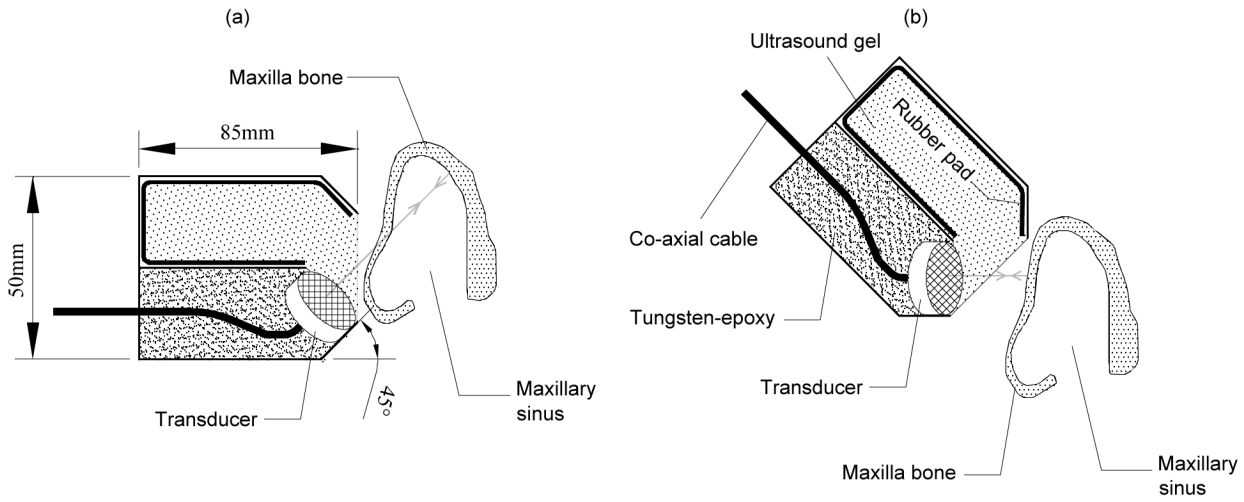

Fig. 9.

Orientations of the transducer for the echo measurements with (a) shear and (b) longitudinal propagations. Sagittal view of the maxilla bone is shown and the skull was upside down.

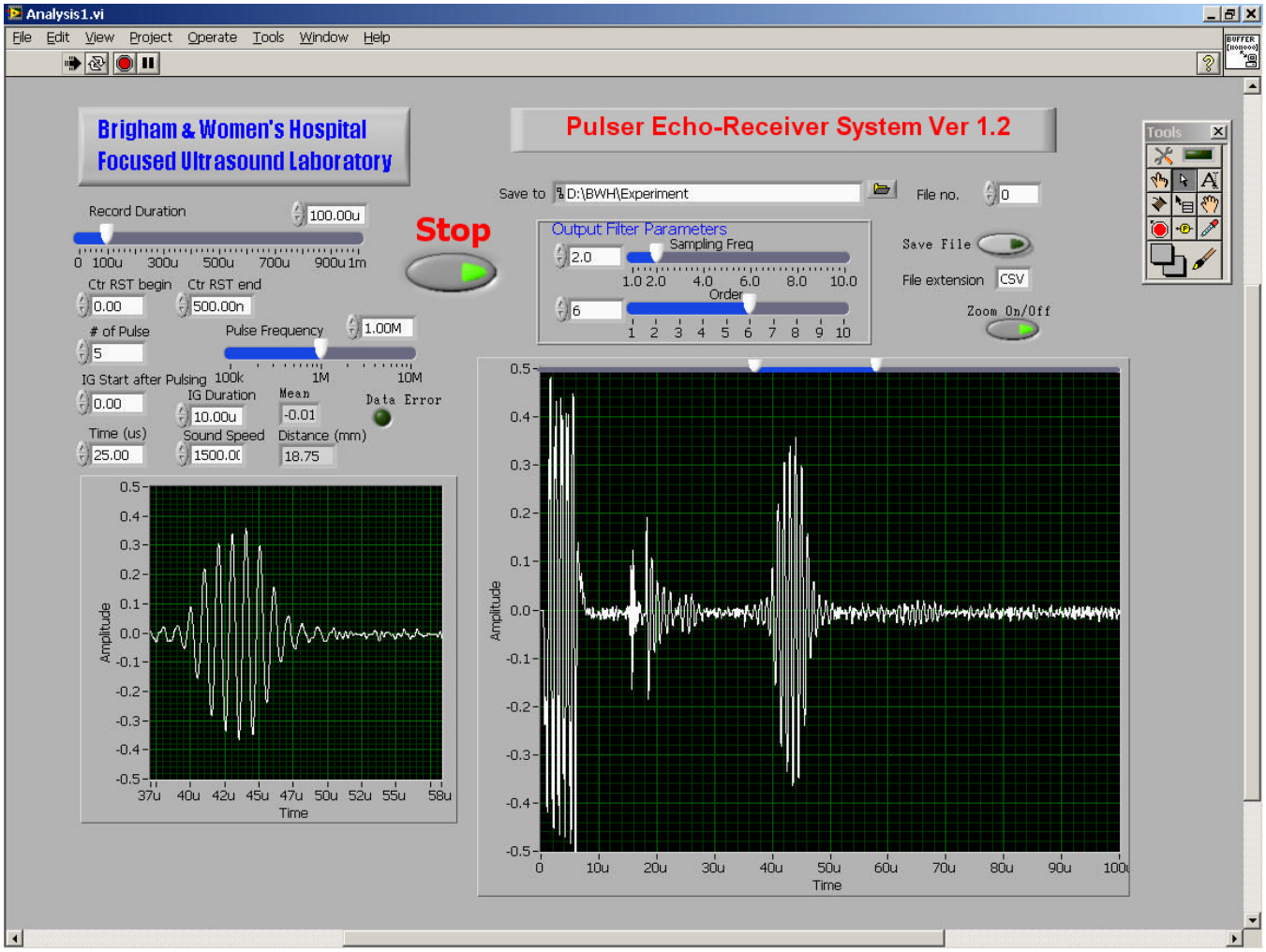

Fig. 10.
Software front panel for the pulser-receiver system.

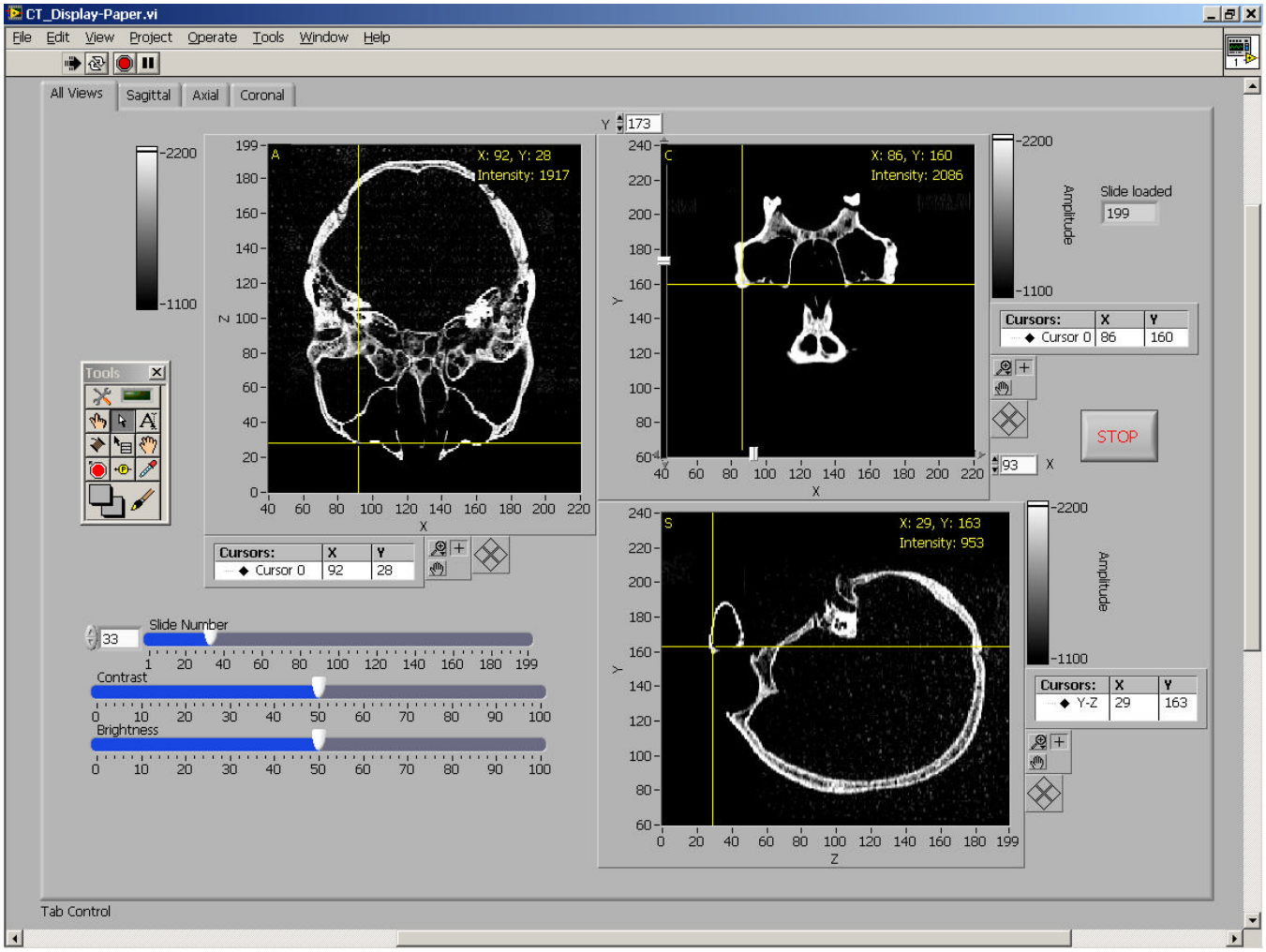

Fig. 11.

Software front panel showing the axial, sagittal and coronal views of the human skull used in the fluid detection experiment.

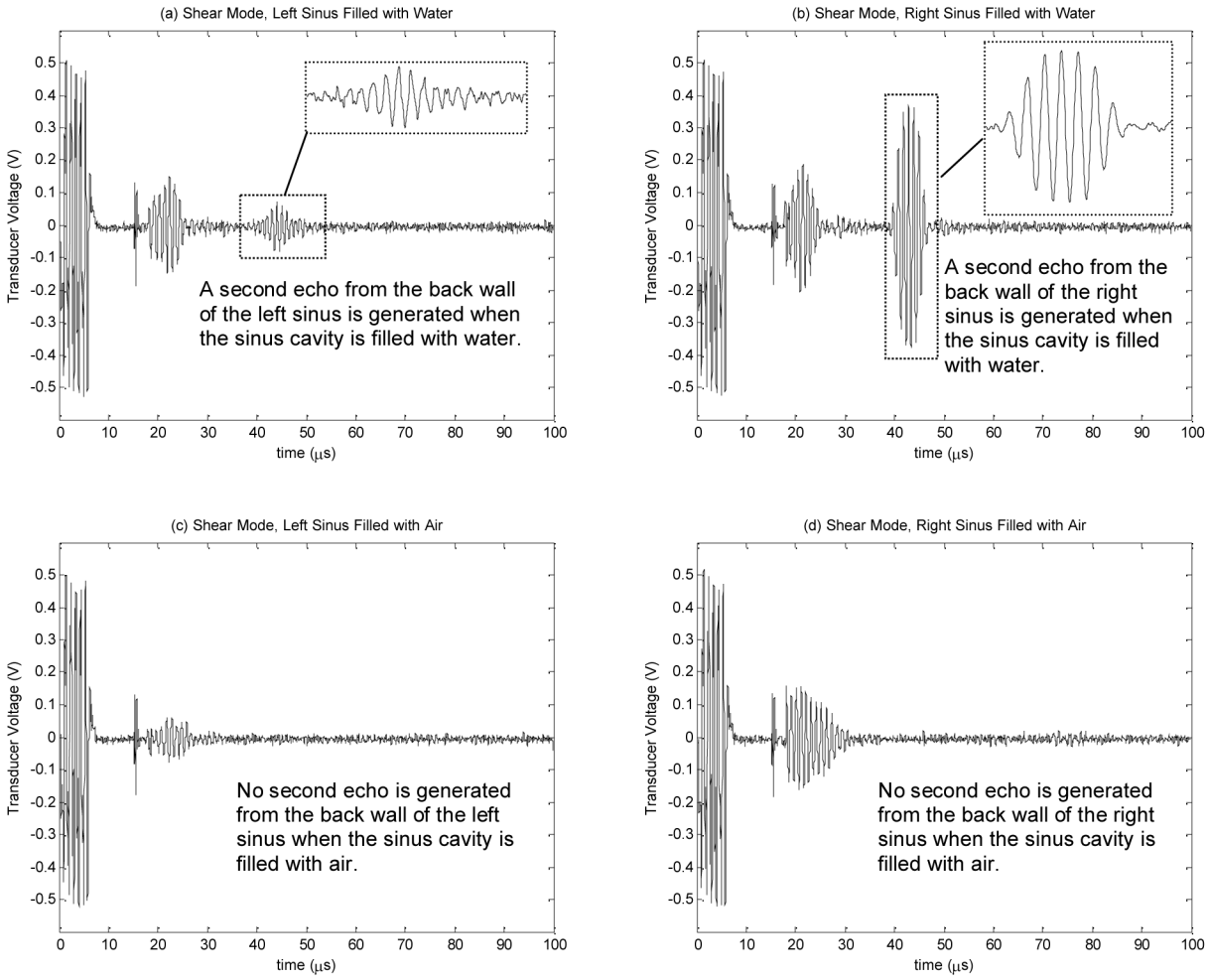

Fig. 12.

Measured transducer voltage for shear propagation in bone: (a) left sinus filled with water, (b) right sinus filled with water, (c) left sinus filled with air, and (d) right sinus filled with air

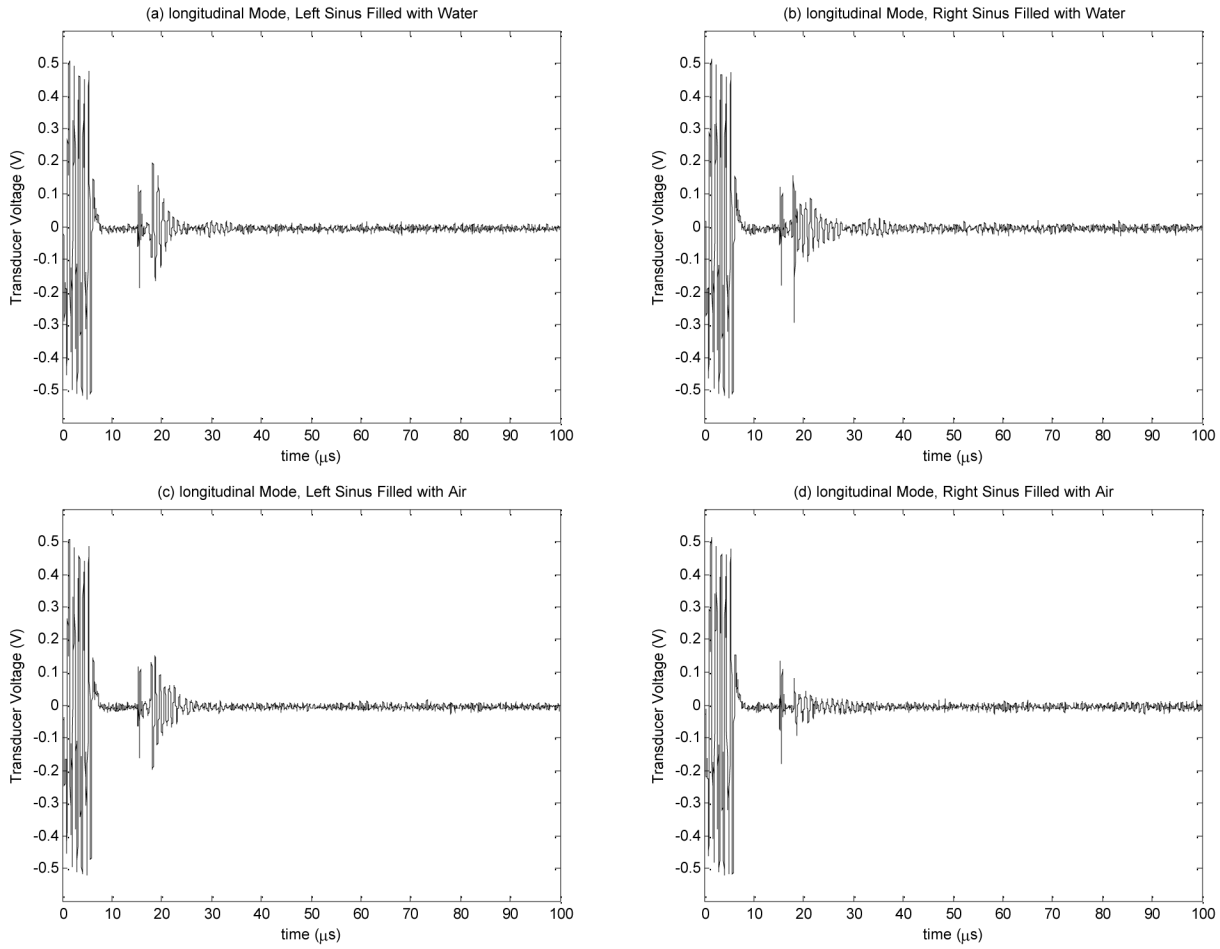

Fig. 13.

Measured transducer voltage for longitudinal propagation in bone: (a) left sinus filled with water, (b) right sinus filled with water, (c) left sinus filled with air, and (d) right sinus filled with air

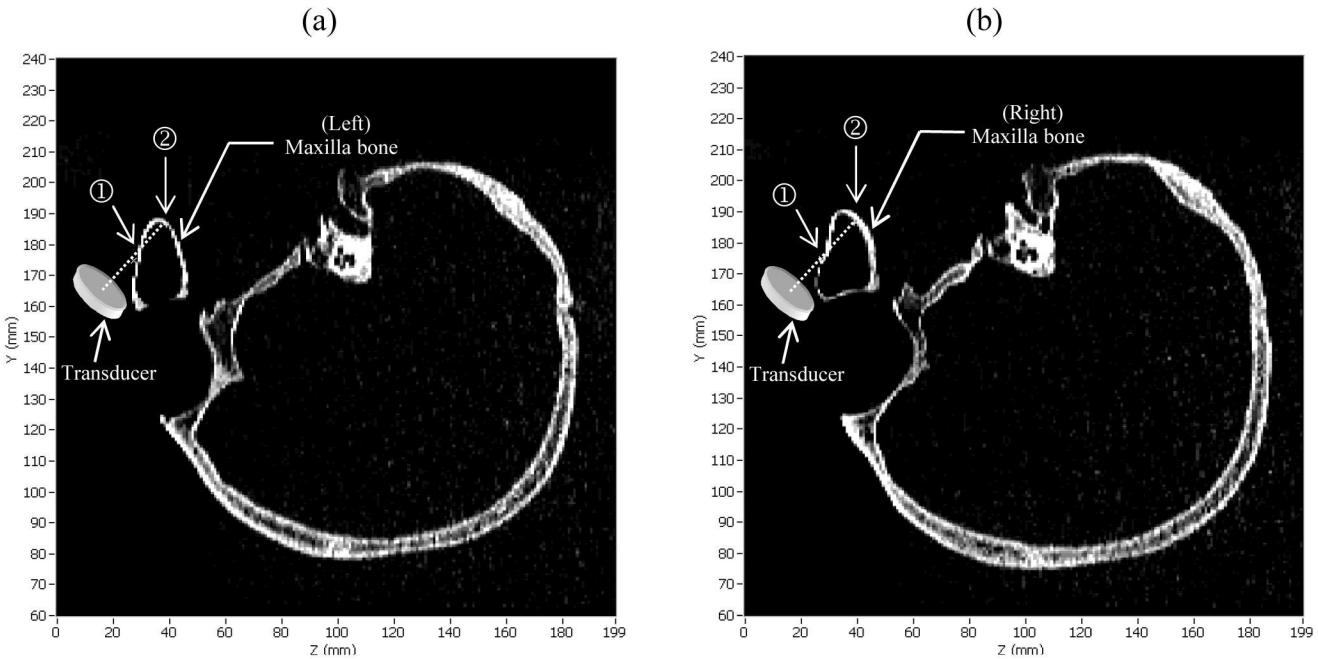

Fig. 14.

Sagittal CT images of the skull (upside down), with indication of the transducer position for shear propagation, showing the (a) left and (b) right maxillary sinuses of the *ex vivo* human skull used in the sinus fluid detection experiment.